ISSN: 0976-3031

*Available Online at http://www.recentscientific.com*

**CODEN: IJRSFP (USA)**

*International Journal of Recent Scientific Research*
*Vol. 10, Issue, 04(B), pp. 31756-31762, April, 2019*

**International Journal of Recent Scientific Research**

**DOI: 10.24327/IJRSR**

**Research Article**

# EFFECT OF TIN PRECURSOR CONCENTRATION ON PHYSICAL PROPERTIES OF SPRAY DEPOSITED TIN SULFIDE THIN FILMS

**Anitha Ezhil Mangaiyar Karasi A[1]., Seshadri S[2] and Amalraj L[3]**

[1]Department of Physics, Shrimati Indira Gandhi College, Trichy, India
[2] Department of Physics,Urumu Dhanalakshmi College, Trichy,India
[3]Department of Physics, V. H. N. S. N. College (Autonomous), Virudhunagar, India

**DOI: http://dx.doi.org/10.24327/ijrsr.2019.1004.3330**

**ARTICLE INFO**

***Article History:***
Received 4th January, 2019
Received in revised form 25th February, 2019
Accepted 18th March, 2019
Published online 28th April, 2019

***Key Words:***

Chemical Spray Pyrolysis , Tin Sulphide XRD,Structural Properties,Optical Properties, Hall Effect

**ABSTRACT**

Tin sulfide thin films were prepared with different molarities of tin species (MSn) at the optimized substrate temperature using the Spray pyrolysis technique to obtain better crystallinity with mono phase thin films. The concentration of Tin II chloride di hydrate precursor is varied from 0.05 to 0.25 ($SnCl^2.^2H^2O$: thiourea) to achieve correct stoichiometry and to tune the concentration of Tin ions in the SnS thin films. These films were well adherent, uniform, and shiny. Lower concentrations of Tin yields highly textured SnS thin films with (111) crystallite orientation. On increasing the concentration, the multi-phases ($SnS^2$ and $Sn^2S^3$) were found to be present along with SnS material. The needle like grains were observed from SEM analysis in these SnS films. Interference effects were predominant in all these thin films in the wavelength region of 400–1100 nm. The direct optical band gap of tin sulfide thin films had decreased from 1.8 eV to 1.55 eV with an increase in MSn from 0.05 to 0.2 M, respectively and further increased to 1.755 eV for 0.25 M concentration. Using Hall Effect measurement, the type of semiconductor is found to be of p-type. A minimum resistivity value of $2.19 \times 10^3$ Ω cm was obtained for the film grown at Msn = 0.2 M.



## INTRODUCTION

Semiconductor thin films have fascinating application in the field of photovoltaic energy conversion [1–3]. Tin sulfide is IV-VI class of compound forming a multiplicity of phases such as SnS, $SnS_2$, $Sn_2S_3$, $Sn_3S_4$, etc. due to their varying coordinating characteristics of tin and sulfur. Amongst these semiconductors, tin sulfide (SnS) has NaCl type structure. Thin film of tin sulfide is composed of sheets of tin atoms and sheets of sulfur atoms [4] and has many properties like high optical absorption co-efficient ($>10^4$ $cm^{-1}$) in the visible region [5], p-type electrical conductivity [6,7], wide optical band gap [8], etc. These properties support the use of this material as a window layer in thin film solar cells [9]. Ozin and co-workers [10] reported that excellent gas sensors can be fabricated for sensing $NH_3$, $H_2S$ or alcohols with nanoporous SnS.

Thin films of SnS were fabricated by various techniques like close-spaced sublimation [11], sulphurization of metallic precursors [12], atmospheric pressure chemical vapor deposition [13], chemical vapor transport [14], chemical deposition [15], vacuum evaporation [16,17], dip coating [18,19], solvothermal process [20], chemical spray pyrolysis [21,22] and each method has its own characteristic advantages and drawbacks in producing homogeneous and defect free thin film. Among them, spray pyrolysis method is principal to prepare tin sulfide thin film, which is a low-cost method that can be used to coat uniform deposition on large surface area [23] with less solution wastage. Since this new spray pyrolysis method is capable of producing mist like sprayed particles of the precursor solution, nanostructured morphological surface with distinct semiconductor properties were anticipated. In the present study, it is desired to prepare and characterize tin sulfide thin films on amorphous glass substrates at different Tin ($M_{Sn}$) precursor concentrations using the precursor solutions of Tin II chloride di hydrate and thiourea by spray pyrolysis technique. As the substrate temperature was optimized earlier, these films of SnS were prepared at that substrate temperature by changing the concentration of both cation and anion precursor solutions, keeping the ratio of precursors of cation and anion species as 1:1 always.

### *Experimental Details*

Tin sulfide thin films were deposited onto amorphous glass substrates with different precursor concentrations of tin species

**Corresponding author:* **Anitha Ezhil Mangaiyar Karasi A**
Department of Physics, Shrimati Indira Gandhi College, Trichy, India

by spray pyrolysis technique. The ratio of molarities of thiourea solution was kept constant at 0.2 M. A detailed description of the mechanism of spray pyrolysis method has been given by Amalraj *et al*. [24]. The precursor solutions of tin II chloride di hydrate ($M_{Sn}$) ($SnCl.^2H_2O$) and thiourea ($M_S$) ($CS(NH_2)_2$) were prepared separately using a solvent containing de-ionized water and isopropyl alcohol in 1:1 ratio, respectively. Two drops of concentrated hydrochloric acid were added for complete dissolution. An equal volume of Tin II chloride di hydrate and thiourea solutions were mixed together and sprayed onto the hot glass substrates with an area of 75 × 24 $mm^2$. The deposition parameters like the substrate temperature, carrier gas pressure, volume of the solution, and nozzle to substrate distance were fixed as 325° C, 0.8 $Kg/cm^2$, 40 ml and 1 cm, respectively. After deposition of these films, it was allowed to cool to room temperature, cleaned with distilled water, dried and then stored in a desiccator.

The crystal structure of these films was examined by the X-ray diffraction (XRD) pattern recorded using XPERT PRO diffractometer using Cu Kα radiation (k = 1.5406 Å). The scanning angle 2θ was varied in the range of 10–60° in steps of 0.05°. The absorption spectrum was recorded in the wavelength range 350–1100 nm using Shimadzu-UV 1800 model double beam spectrophotometer. Photoluminescence emission spectra of the as-deposited samples were obtained using a HITACHI F 7000 Fluorescence spectrophotometer. The surface morphology of the as-deposited SnS thin films was recorded with a magnification of about 20,000 by CARLZEISS (EV018) scanning electron microscope with a working distance of around 10 mm and the chemical composition of the films was recorded with the same instrument. The room temperature mobility, Hall co-efficient and effective carrier concentration were determined using an automated Hall Effect system (ECOPIA HMS – 3000) with Vander paw configuration. The activation energy values were calculated using the conventional four probe method in the temperature range 40–100°C

## RESULTS AND DISCUSSION

The color of the thin film prepared with 0.05 M concentration was pale golden yellow with less adhesion to the substrate. Thin films prepared with 0.1 M, 0.15 M, and 0.2 M concentrations had good adherence and were gray in color. These films looked shiny with multiple colors due to internal multiple reflections and dark gray in color due to transmitted light. For 0.25 M concentration, the film appeared with brown color along the edges of the film and with a dark gray in the middle with good adhesion. This variation in the color may be due to light variation in the temperature of the substrate which may be evident and prominent at higher concentration. The thickness values were determined as 300, 350, 410, 555, and 520 nm for the samples prepared with the tin precursor concentrations of 0.05, 0.1, 0.15, 0.2, and 0.25 M, respectively.

### *Structural Studies*

The XRD profiles of these five samples are shown in Figure 1. From the XRD profiles, all the SnS thin films showed a broad peak around 31.7° with a preferential orientation along (111) plane revealing the polycrystalline nature having the Orthorhombic structure. The peaks corresponding to other planes of SnS were not observed, indicating these SnS films were highly textured. This (111) orientation was matched well with the JCPDS file no-39-0354. The low intensity diffraction peak was observed around 31.7° at the precursor concentration of 0.05 M. The intensity of diffraction peak shows polycrystalline phase became more intense and sharp with the increase in precursor concentration up to 0.2 M, which shows an enhancement of the crystallinity of the layers. Above this precursor concentration, the peak intensity of the (111) is reduced and other peaks corresponding to $Sn_2S_3$ and $SnS_2$ materials such as 21.33° (110) and 14.88° (001), respectively, started to appear. At higher precursor concentration of tin species, the presence of multi-phases ($Sn_2S_3$ and $SnS_2$) along with SnS phase might be due to less availability of sulfur atoms. These peaks are in good agreement with the standard JCPDS card No-72-0031 ($Sn_2S_3$) and 23-0677 ($SnS_2$). At higher precursor concentration of 0.25 M, growth in the surface of the substrate and leads to the nonlinear growth in this precursor concentration leads to the homogeneous reaction which in turn leads to the peeling of the films, therefore the thickness with precursor concentration can attributed to the decrease in intensity of (111) peak.

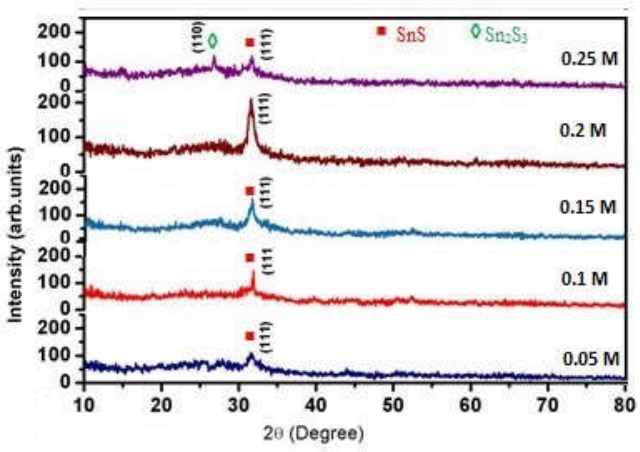


**Figure 1** XRD of SnS thin films with different precursor concentrations.

From the XRD pattern of all the SnS films, the peak slowly increased with the increase in precursor concentration of 0.2 M, the peak fully disappeared and started to appear for further increase in precursor concentration. The hump of SnS film was formed due to X-rays reflected from the amorphous glass substrates. From the XRD profiles, it was concluded that single face material of SnS could be prepared with cation precursor concentration in the range of 0.05 to 0.2 M, the latice parameter values of the peak were determined from the orthorhombic structure these values were comparable with JCPDS standard data (JCPDS card No.39-0354).

The peak position (2θ), FWHM values and stacking fault probability (α*) present in all the samples were calculated and listed in table. 1. The crystallite size was determined using the Debye Scherrer's formula [25].

$$D = \frac{k\lambda}{\beta \cos \theta}$$

Where, k is a constant (0.94) , $\beta$ is the Full Width Half Maxium value, $\lambda$ is the wavelength of a Cu-$k_\alpha$ radiation source ($\lambda$=1.5418Å) and $\theta$ is the Bragg angle. The strain

present in the SnS thin films ($\varepsilon$) was calculated the using relation [26].

$$\varepsilon = \frac{\beta \cos\theta}{4}$$

The dislocation is an irregularity in the crystal structure. It can strongly affect many properties of the materials. Crystalline materials contains periodic sturcture with the molecules or atoms placed in repeating fixed positions and this periodicity can be determined by the unit cell parameters. The dislocation or the crystallographic defects interrupt the regular periodic lattice structure. The dislocation density (δ) can be evaluated using relation [27].

$$\delta = \frac{1}{D^2}$$

The stacking fault probability (α*) is a fraction of layers that undergo stacking sequence faults in a given crystal. The stacking fault probability affect the optoelectronic properties of the films due to the distorted lattice and was determined using the relation [28]

$$\alpha^* = \left( \frac{2\Pi^2}{45(3\tan\theta)^{\frac{1}{2}}} \right) \beta$$

The sizes of the crystallites in all the cases are found to be in nano range (5nm-35nm) and these nanocrystallites explain that the SnS thin films have larger nucleation rate than the growth rate due to more number of nucleation centers that exist on the substrate surface [29]. The size of the SnS crystallites found to increase from 5 nm to 35 nm with the increase in precursor concentration from 0.05 to 0.2M. The increase in crystallite size may be attributed to the improvement of the crystallinity and an increase in the cluster formation owing to increase of precursor concentration leading to agglomeration of small crystallites. These agglomerated crystallites combine together, resulting in the formation of larger crystallites with better crystallinity. The crystallite size decreased to 13 nm when the precursor concentration was increased up to 0.25 M, where the decrease may be due to the lesser thickness corresponding to 0.2 M film thickness and hence less agglomeration among them. Kherarchi *et al*. [30] had reported the similar crystallite size values (12.35nm-16.98nm) on the influence of various tin molarities for SnS thin films prepared by an ultrasonic spray technique. The crystallite size of the SnS can be affected by so many factors such as impurities, defects, and heating conditions. Figure 2 shows the variation in the crystallite size, strain, and dislocation density of the films as a function of precursor concentrations. The lattice strain, dislocation density, and stacking fault probability of the films decreases with an increase in precursor concentration up to 0.2 M and is increased for further increasing of molar concentration. From

**Table 1** Variation of structural and elemental properties of SnS thin films with different precursor concentration.

| | | | | | Elemental composition | | |
|---|---|---|---|---|---|---|---|
| Precursor concentration (MSn) | Peak position 2θ (degree) | FWHM | Crystallite size (nm) | Stacking fault (×10−3 J/m2) | Sn (at.%) | S (at.%) | Sn/S ratio |
| 0.05 | 31.7662 | 0.4920 | 11.9 | 20.82 | 50.5 | 49.5 | 1.02 |
| 0.1 | 31.7710 | 0.4920 | 17.5 | 9.5 | 52.2 | 47.8 | 1.12 |
| 0.15 | 31.7847 | 0.4920 | 19 | 5.5 | 56.3 | 46.7 | 1.14 |
| 0.2 | 31.7932 | 0.3936 | 29.2 | 4.1 | 53.9 | 46.1 | 1.17 |
| 0.25 | 31.6292 | 0.5904 | 14.6 | 8.6 | 54.4 | 45.6 | 1.19 |

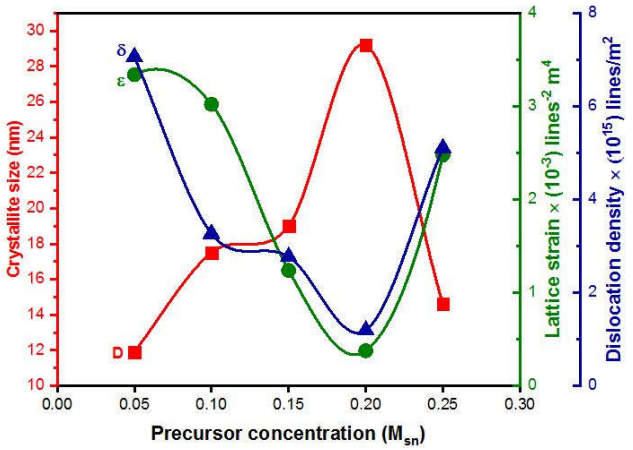


**Figure 2** The variation of structural parameters with different tin concentration of SnS thin films

these observations, it is clear that when the precursor concentration of tin increases, the crystallite size increases and this leads to a decrease in grain boundaries, lattice strain, dislocation density, and stacking fault probability. The decrease in grain boundaries at higher precursor concentration (0.2 M) indicates the reduction of crystal lattice imperfections and formation of high-quality films.

### *Surface Morphology*

The surface morphology of tin sulfide thin films was grown by spray pyrolysis technique with different tin precursor concentrations and was characterized and analyzed by photographing the scanning electron microscope images as shown in Figure 3. These SEM photographs were recorded with magnifications of about 20,000. The SEM images show that the surface morphology strongly depends upon molar concentrations of the tin species solutions. For the films formed with the molar concentrations of 0.05–0.2 M, the solution droplets containing tin chloride and thiourea reach the substrates where the evaporation of solvent occurs thereby forming a solid phase of SnS in the form of thread-like crystallites. The needle-shaped grains of SnS were spread homogeneously over the surface of the films. It has been observed that needle-shaped SnS grains are found to increase in size with an increase in precursor concentrations. The definite and well-grown plate like formation of grains was observed for the film prepared with the precursor concentration of 0.2 M. Similar needle-shaped grains for SnS films were observed in the earlier reports [13,31,32]. However, the surface morphology of the film prepared

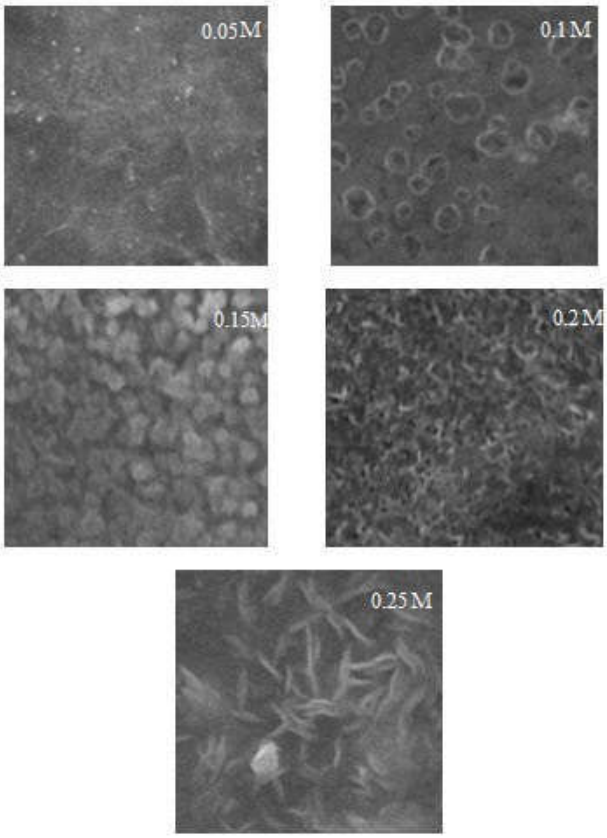


**Figure 3** SEM images of SnS thin films with different precursor concentrations.

with the precursor concentration of 0.25 M is distinctly different from other SEM images. The high density of clusters or heaps was randomly distributed on the surface of the film at the higher precursor concentration of tin species due to faster nucleation and their grain boundary not being clearly visible. When increasing the precursor concentration from 0.2 to 0.25 M, there is a lower probability of rearrangement of the arriving material and the inhomogeneity increases inducing the formation of clusters [33]. Such morphology may be due to the presence of multiphase ($SnS_2$ and $Sn_2S_3$) material along with SnS material which was evident from the XRD analysis discussed earlier.

EDAX spectrum of tin sulfide thin film prepared with the precursor concentrations of 0.05-0.25 M was recorded in the binding energy region of 0.5– 13.0 KeV as shown in Figure 5. The atomic percentage of tin and sulfur was observed as 50.5% and 49.5%, respectively, for the first sample (0.05 M). The atomic percentage of sulfur had decreased from 49.5% to 45.6% when increasing the precursor concentrations from 0.05 to 0.25 M, respectively. The nearly correct stoichiometric ratio of 49.5:50.5% was observed for tin and sulfur at the precursor concentration of 0.2 M. For 0.25 M precursor concentration, the atomic percentage of tin and sulfur was observed as 54.4 and 45.6 %, respectively, which predicts the mixed phases of $SnS_2$, $Sn_2S_3$, and SnS present in this film prepared with a precursor concentration of 0.25 M. The changes observed in the stoichiometric ratio with precursor concentration were also supported by the structure analysis and surface morphology. Variations of tin and sulfur percentage with different precursor concentrations were listed in Table 1.

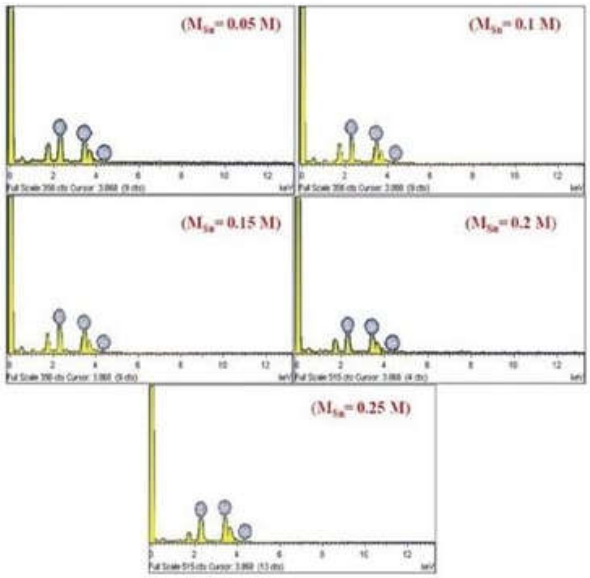


**Figure 4** EDAX images of SnS thin films with different precursor concentrations.

### *Optical Properties*

The optical transmittance spectra obtained from the recorded absorption spectra of the as grown SnS thin films prepared with different tin precursor concentrations are shown in Figure 5. The multiple interference effect was observed for all the five samples in the wavelength region of 400–1100 nm, which confirms the formation of uniform and smooth films.

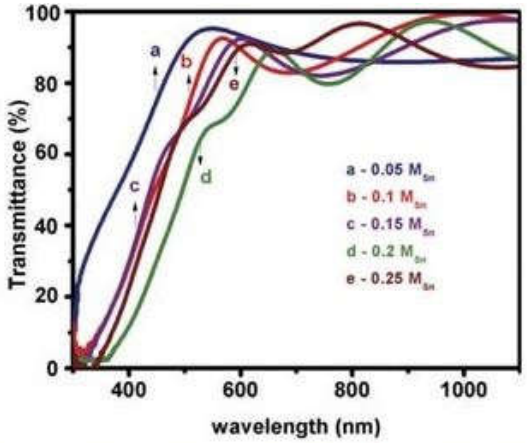


Figure5 . A plot of transmittance spectra of SnS thin films with different concentrations of tin species.

Below 600 nm, multiple interference effect was not predominant in all the films, which may be due to the absorption of such photons and hence the absence of coherence [6].

The transmittance value of all the SnS films is in the visible region and it decreased with an increase in precursor concentration from 0.05 M to 0.2 M and with further increase in the precursor concentration to 0.25 M, the transmittance had increased. The decrease in transmittance may be attributed to the increase in film thickness which leads to an inversion in loss of intensity due to absorption and scattering.

Thus the absorption coefficient "α" of the SnS thin film was calculated in the visible region using thickness "t" and the

absorption spectrum. The variation of "α" with wavelength is plotted for these SnS thin films as shown in Figure 6. The calculated absorption coefficient value for SnS films exceeds $10^4$ $cm^{-1}$, which indicates that the layers were with high absorption value. Hence, the layers might be suitable for photo voltaic devices [35]. The absorption is more for high-energy photons in the recorded region for this SnS material. A similar absorption coefficient value had been reported by Wang *et al*. [31].

The optical band gap ($E_g$) can be determined from the absorption coefficient (α) and photon energy (hυ) by the equation.

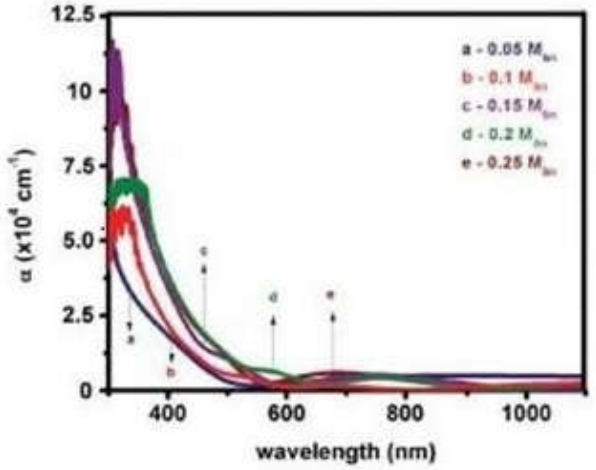


Figure 6 . A plot of absorption co-efficient with wavelength of SnS thin films with different precursor concentrations of tin species.

$$(\alpha h\nu) = A(h\nu - E_g)^P$$

Where A is a constant, h is planck's constant, ν is the frequency and p has $2, 3, \frac{1}{2}$ *and* $\frac{3}{2}$ values for allowed indirect, forbidden indirect, allowed direct and forbidden direct transissions respectively . A graph was plotted against $(\alpha h\nu)^2$ and photon energy (hν) as shown in Figure. 8. The straight line portion was extrapolated to photon energy axis to give bandgap $E_g$. The direct optical bandgap of SnS thin films were founded to be 1.78, 1.76, 1.75, 1.74 and 1.755 eV respectively coresponding to increase in precursor concentrations from 0.05 M to 0.25 M. Fadavieslam *et al* [36] had reported similar direct optical bandgap values from 1.63 to 1.81 eV for SnS thin films as a function of deposition conditions on the physical properties by spray pyrolysis method. Kherchachi [30] had studied the same energy bandgap value ranged from 1.23 to 1.8 eV for SnS thin films grown by ultrasonic spray pyrolysis method. The direct optical bandgap values decreased to a minium of 1.23 eV at 0.2 M with an increase in precursor concentration from 0.05 M and with futher increase in the precursor concentration to 0.25 M, the bandgap value had increased to 1.8 eV respectively. Generally the decrease in optical bandgap may be attributed to the increase in crystllite size [37], thickness and crystallinity[38], roughness and grain size. In the present study it is believed that increase in crystallite size and crytallinity is accountable for the decrease in the bandgap, which is evidenced by XRD results. The increase in bandgap at 0.25 M can be attributed to the decrease in thickness and crystallite size at that concentration comparing to 0.2 M, leading to its corresponding electronic structure. Since, the peak heights corresponding to $SnS_2$ and $Sn_2S_3$ phases are very small compared to that of SnS, the presnce of those materials corresponding to the two phases other than SnS will be very small. The bandgap of values of $Sn_2S_3$ and $SnS_2$ are of the order of 1.64 eV [39] and 2.75 eV [40], respectively. The 1.755 eV bandgap of 0.25 M film is more than that of 0.2 M (1.75 eV). This shows that the presence of other two phases does not have any influence on the band gap of SnS.

In general, the luminesence property of the films has a close relation with the film crystallinity because the density of the defects in film reduces with an improvement of the crytallinity. The PL emmission spectrum for all the samples was measured innthe wavelength range of 650 to 750 nm at an excitation wavelength of 450 nm. PL spectra of SnS thin films deposited at various Sn molarities are sholwn in Figure 9. All the SnS films exhibit a strong luminescence peak near band edge emmissions (NBE) at 755 nm (1.75 eV) (blue) due to recombination of bound excitons. All the films show only the NBE peak in the visible region and IR and UV emmission peaks were not observed in these films idicating a good optical quality of the films.

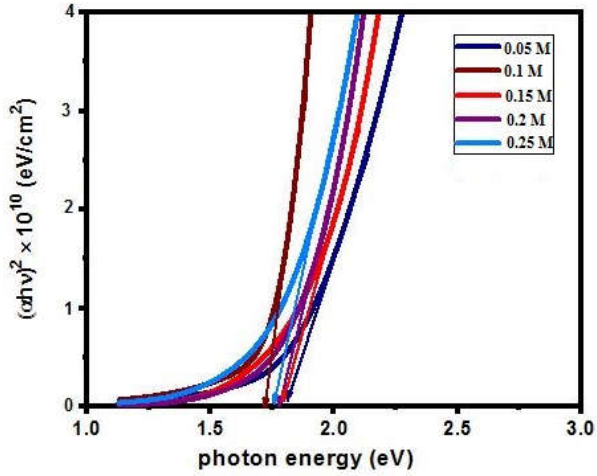


**Figure 7** The $(\alpha h\nu)^2$ versus hν curves for the optical band gap determination of SnS thin films at different concentration of tin species.

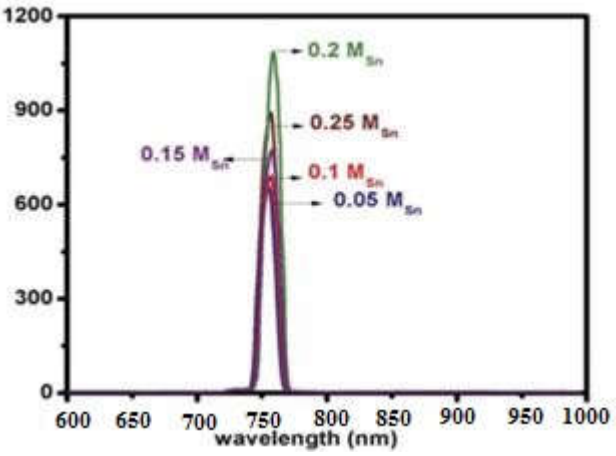


**Figure 8** PL spectra of SnS thin films with different precursor concentrations of tin species.

It is seen from the figure that the NBE emission peak very slightly shifted toward higher wavelength side when the precursor concentration is increased up to 0.2 M and with further increasing the precursor concentration it shifted toward lower wavelength side. This result is well matched with the optical band gap values. This result reveals that the peak is maximum for the sample prepared with the precursor concentration of 0.2 M. The single emission peak in the present study may indicate the compound SnS prepared by this nebulized spray pyrolysis technique is free from above defects like sulfur vacancies and interstitials tin atoms. It reveals the fact that no impurity levels or defect levels were present within the forbidden band gap. Wang *et al*. [41] had reported the PL emission peak at 420 nm for the SnS nanocrystallites. The gradual increase in peak intensity was observed with increasing the precursor concentration up to 0.2 M. The increase in peak intensity with an increase in precursor concentrations indicated the development in crystalline quality and hence an increase in density of free excitons [42]. The decrease in peak intensity was observed in PL spectra when the precursor concentration increased up to 0.25 M. As the thickness decreases, the number of molecules and hence the population will decrease which in turn decreases the peak height.

***Electrical Properties***

The electrical resistivity, carrier concentration and Hall coefficient of SnS thin films grown at different precursor concentrations were determined by Hall Effect measuring instrument at room temperature and the corresponding values are given in Table 2. The resistivity of the SnS thin films decreases from 585 × $10^3$ Ω cm to 2 × $10^3$ Ω cm with the increase in precursor concentration from 0.05 M to 0.2 M. The decrease in resistivity may be attributed to the increase in crystallite size which leads to a decrement in the trapping states at grain boundary [43]. The grain boundary plays an important role between the crystallites and the carrier transport. It can act as a trap center in an incomplete atomic bonding, which depletes the free charge carriers and as a resultant, more number of free carriers become immobilized as trapping state increase. The resistivity again increases to 9 × $10^3$ Ω cm, while the precursor concentration had increased to 0.25 M. These thin films are found to exhibit n-type electrical conduction. The Hall mobility and bulk carrier concentration increases with increase in precursor concentration up to 0.2 M and decreases with the further increase in precursor concentration.

## CONCLUSION

SnS thin films were prepared with different precursor concentrations of tin species from 0.05 M to 0.25 M (in steps of 0.05 M) by spray pyrolysis technique successfully. The ratio of Thiourea solution was kept constant at 0.1 M. The as-deposited SnS thin films were smooth, shiny, adherent, and dark brown in color. XRD studies showed polycrystalline nature of the films having orthorhombic structured crystallites with the preferential orientation of (111) plane for the above precursor concentrations. For the precursor concentration of 0.25 M, mixed phases of Hexagonal and Orthorhombic were present. Direct allowed optical band gap was found to be present in all these SnS thin films, which may be suitable for preparing better quality solar cells. The surface morphology of SnS thin films was defined with needle-like structure. The EDAX result revealed the exact stoichiometry for the SnS film prepared with the precursor concentration of 0.2 M. The electrical resistivity of SnS thin films had been decreased by increasing the precursor concentration from 0.05 to 0.2 M. A minimum electrical resistivity was observed as 2.19 × $10^3$ Ω cm for the precursor concentration of 0.2 M. These thin films were found to exhibit p-type electrical conduction. From the above results, it can be concluded that this tin sulfide thin film is a good candidate for the fabrication of solar cell and photo detector devices.

**Table 2** The optical and electrical parameters of SnS thin films with different precursor concentrations of tin.

| Precursor concentration (MSn) | Thickness (nm) | Band gap (eV) | Resistivity (×$10^3$ Ω cm) | Carrier concentration (×$10^{13}$ cm−3) | Mobility ($cm^2$/ Vs) | Hall coefficient (×$10^5$ $cm^3$/c) |
|---|---|---|---|---|---|---|
| 0.05 | 299 | 1.78 | 90.82 | 1.124 | 6.114 | −5.55 |
| 0.1 | 338 | 1.76 | 18.24 | 1.974 | 17.33 | −3.16 |
| 0.15 | 410 | 1.75 | 10.08 | 2.600 | 23.81 | −2.41 |
| 0.2 | 555 | 1.74 | 2.192 | 7.683 | 37.15 | −0.82 |
| 0.25 | 520 | 1.755 | 9.027 | 2.172 | 31.83 | −2.87 |

## References


1. Noguchi H, Setiyadi A, Tanamura H, *et al*. Characterization of vacuum-evaporated tin sulfide film for solar cell materials. Sol Energy Mater Sol Cells. 1994;35:325–331.
2. Ristov M, Sinadinovski G, Grozdanov I. Chemical deposition of tin sulphide thin films. Thin Solid Films. 1989;173:53–58.
3. Acharya S, Srivastava ON. Electronic behavior of SnS crystals. Phys Status Solidi. 1981;65:717–723.
4. Greenaway DL, Nitsche R. Preparation and optical properties of group IV-$VI_2$ chalcogenides having the $CdI_2$ structure. Phys Chem Solids. 1965;26:1445–1458.
5. Thangaraju B, Kaliannan P. Spray pyrolytic deposition and characterization of SnS and $SnS_2$ thin films. J Phys D Appl Phys. 2000;33:1054–1059.
6. Amalraj L, Sanjeeviraja C, Jayachandran M. Spray pyrolysized tin sulphide thin films and characterization. J Cryst Growth. 2000;234:683–689.
7. Deshpande NG, Sagade AA, Gudage YG, *et al*. Growth and characterization of tin sulfide (SnS) thin film deposited by successive ionic layer adsorption and reaction (SILAR) technique. J Alloys Compd. 2007;436:421–426.
8. Sankapal BR, Mane RS, Lokhande CD. Successive ionic layer adsorption and reaction (SILAR) method for the deposition of large area (~10 $cm^2$) tin sulfide (SnS) thin films. Mater Res Bull. 2000;35:2027–2203.
9. Shi C, Chen Z, Shi G, *et al*. Influence of annealing on characteristics of tin sulfide thin films by vacuum thermal evaporation. Thin Solid Films. 2012;520:4898–4901.
10. Ozin GA, Jiang T, Verma A, *et al*. Absorption and sensing properties of micro porous layered tin sulfide materials. J Mater Chem. 1998;8:1649–1656.
11. Shi C, Yang P, Yao M, *et al*. Preparation of $SnS_2$ thin films by closed space sublimation at different source temperature. Thin Solid Films. 2013;534:28–31.
12. Malaquias J, Fernandes PA, Salomé PMP, *et al*. Assessment of the potential of tin sulphide thin films

prepared by sulphurization of metallic precursors as cell absorbers. Thin Solid Films. 2011;519:7416–7420.
13. Price LS, Parkin IP, Hardy AME, *et al*. Atmospheric pressure chemical vapor deposition of tin sulfides (SnS, $Sn_2S_3$, and $SnS_2$) on glass. Chem Mater. 1999;11:1792–1799.
14. Matsumoto K, Takagi K. Chemical transport of $SnS_2$ using sulfur as a transporting agent. J Cryst Growth. 1983;63:202–204..
15. Lokhande CD. A chemical method for tin disulphide thin film deposition. J Phys D Appl Phys. 1990;23:1703–1705.
16. Kawano K, Nakata R, Sumita M. Effects of substrate temperature on absorption edge and photocurrent in evaporated amorphous $SnS_2$ films. J Phys D Appl Phys. 1989;22:136–141.
17. George J, Joseph KS. Absorption edge measurements in tin disulphide thin films. J Phys D Appl Phys. 1982;15:1109–1116.
18. Panda SK, Antonakos A, Liarokapis E, *et al*. Optical properties of nanocrystalline $SnS_2$ thin films. Mater Res Bull. 2007;42:576–583.
19. Sekar Ray C, Karanjai MK, Das Gupta D. Structure and photoconductive properties of dip-deposited SnS and $SnS_2$ thin films and their conversion to tin dioxide by annealing in air. Thin Solid Films. 1999;350:72–78.
20. Hai B, Tang K, Wang C. Synthesis of $SnS_2$ nanocrystals via a solvothermal process. J Cryst Growth. 2001;25:92–95.
21. Khélia C, Boubaker K, Nasrallah TB. Morphological and thermal properties of β-$SnS_2$ sprayed thin films using Boubaker polynomials expansion. J Alloys Compd. 2009;477:461–467.
22. Vijayakumar K, Sanjeeviraja C, Amalraj L. Characterization of tin disulphide thin films prepared at different substrate temperature using spray pyrolysis technique. J Mater Sci Mater Electron. 2011;22:929–935.
23. Reddy NK, Reddy KTR. Preparation and characterization of sprayed tin sulfide films grown at different precursor concentrations. Mater Chem Phys. 2007;102:13–18.
24. Raj Mohamed J, Amalraj L. Effect of precursor concentration on physical properties of nebulized spray deposited $In_2S_3$ thin films. J Asian Ceram Soc. 2016;4:357–366.
25. Anitha N, Anitha M, Amalraj L. Influence of precursor solution volume on the properties of tin disulphide ($SnS_2$) thin films prepared by nebulized spray pyrolysis technique. Optik. 2017;148:28–38.
26. Anitha M, Anitha N, Amalraj L. Influence of precursor concentration on physical properties of CdO thin films prepared by spray pyrolysis technique using nebulier. Appl Phys A. 2017;123:764–779.
27. Raj Mohamed J, Sanjeeviraja C, Amalraj L. Influence of substrate temperature on physical properties of (111) oriented $CdIn_2S_4$ thin films by nebulized spray pyrolysis technique. J Asian Ceram Soc. 2016;4:191–200.
28. Anitha M, Anitha N, Amalraj L, *et al*. Investigations on the structural, electrical and optical properties of thin films of $CdO_{(111)}$. J Mater Sci Mater Electron. 2017;28:17297–17307.
29. Rajathi S, Kirubavathi K, Selvaraju K. Structural, morphological, optical and photoluminescence properties of nanocrystalline PbS thin films grown by chemical bath deposition. J Arab J Chem. 2014;11:057–065.
30. Kherchachi IB, Saidi H, Attaf A, *et al*. Influence of solution flow rate on the properties of $SnS_2$ films prepared by ultrasonic spray. Optik. 2016;127:2266–2270.
31. Wang S, Wang S, Chen J, *et al*. Influence of the deposition parameters on the properties of $SnS_2$ films prepared by PECVD method combined with solid sources. J Nanopart Res. 2014;16:2610–2622.
32. Voznyi A, Kosyak V, Opanasyuk A, *et al*. Structural and electrical properties of $SnS_2$ thin films. Mater Chem Phys. 2016;173:52–61.
33. Panda NR, Acharya BS, Nayak P, *et al*. Studies on growth morphology, UV absorbance and luminescence properties of sulphur doped ZnO nanopowders synthesized by the application of ultrasound with varying input power. J Ultrason Sonochem. 2014;21:582–589.
34. Bhushan B, Fuchs H, Tomitori M. Applied scanning probe methods VIII – Scanning probe microscopy techniques. Berlin: Springer; 2008.
35. Ramakrishna Reddy KT, Chalapathy RBV. Structural properties of $CuGa_xIn_{1-x}Se_2$ thin films deposited by spray pyrolysis. Cryst Res Technol. 1999;34:127–132.
36. Fadavieslam MR, Shahtahmasebi N, Rezaee-Roknqgqei M, *et al*. Effect of deposition conditions on the physical properties of SnxSy thin films prepared by spray pyrolysis technique. J Semicond. 2011;32:113002–113008.
37. Jundale DM, Joshi PB, Sen S, *et al*. Nanocrystalline CuO thin films: synthesis, microstructural and opto-electronic properties. J Mater Sci Mater Electron. 2012;23:1492–1499.
38. Liu F, Lai Y, Liu J, *et al*. Characterization of chemical bath deposited CdS thin films at different deposition temperatures. J Alloys Compd. 2010;493:305–308.
39. Srinivasa Reddy T, Santhosh Kumar MC. Effect of substrate temperature on the physical properties of co-evaporated $Sn_2S_3$ thin films. Ceram Int. 2016;42:12262–12270.
40. Srinivasa Reddy T, Santhosh Kumar MC. Co-evaporated SnS thin films for visible light photodetector applications. RSC Adv. 2016;6:95680–95692
41. Wang C, Tang K, Yang Q, *et al*. Raman scattering, far infrared spectrum and photoluminescence of $SnS_2$ nanocrystallites. Chem Phys Lett. 2002;357:371–375.
42. Gowri Manohari A, Santhosh Kumar K, Mahlingam T, *et al*. Buffer layer of antimony doped tin disulfide thin films for heterojunction solar cells. Mater Lett. 2015;155:121–124.